J Solid State Electrochem (2010) 14:139–148
DOI 10.1007/s10008-009-0805-6

ORIGINAL PAPER

Sn–Co–C composites obtained from resorcinol-formaldehyde gel as anodes in lithium-ion batteries

P. Lavela · F. Nacimiento · G. F. Ortiz · J. L. Tirado

Received: 20 January 2009 / Revised: 5 February 2009 / Accepted: 10 February 2009 / Published online: 24 February 2009

Abstract Sn–Co–C composites have been prepared by using the resorcinol/formaldehyde polymerization method combined with the carbothermal reduction of metal oxides during carbonization. Homogeneously dispersed metal/carbon composites were identified by electron microscopy. Scanning electron microscopy images revealed the presence of carbonaceous particles with inclusions of metal agglomerates, and the X-ray diffraction patterns revealed the presence of tin and cobalt–tin phases. The introduction of small amounts of cobalt led to higher capacities as compared to coke and cobalt-free samples. The sample with a Sn/Co molar ratio of 85:15 and a higher, initial metal oxide-to-resorcinol ratio was able to maintain capacity values near 380 mAh/g after 30 cycles. The instability of cobalt–tin phases on cycling was not a hindrance for the electrochemical behavior. Charge transfer resistance values were kept low during cycling for cobalt-containing composites.

Keywords Lithium · Coke · Battery · Mössbauer · Composite

Introduction

At present, the research for new anodes in lithium ion batteries is mature in the field of both carbonaceous materials and metals, such as tin, which are able to form alloys with lithium [1]. Graphite is a preferred option due to the low working voltage and stable capacity for a large number of cycles [2, 3]. On the other hand, the theoretical capacity limit (372 mAh/g) is regarded as a major drawback to develop new batteries with higher capacities in the near future. New approaches are continuously proposed to overcome this limitation including mild oxidation [4] and fluorination [5].

Disordered carbons prepared at low temperatures, as cokes, must not be discarded yet. Their low cost is an advantage for commercial purposes. Also the existence of additional sites for lithium linking, provided by the incomplete structural ordering, is a factor deserving the evaluation of new approaches for their use in lithium ion batteries.

On the other hand, tin metal is able to reversibly react with important amounts of lithium to deliver high capacity. The volume expansion occurring during the reversible alloying process has been attenuated by several means, including preparation of glasses and combination with different counter ions and/or metals [6, 7]. However, a new approach considers the introduction of transition metals, as cobalt, in the anode composition [8]. The lack of reactivity of cobalt metal with lithium prevents the addition of large amounts of this element, which could significantly reduce the electrode capacity. However, it has been reported that small amounts of cobalt contribute to introduce structural disorder in the tin phase. This phenomenon can be envisaged as a beneficial factor for capacity stability [8].

Several methods have been reported to achieve a homogeneous mixture of metal and carbon phases, ensuring a suitable buffering effect of the carbonaceous materials. Milling [9], sputtering [10], or chemical deposition [11] procedures have been employed. Nongraphitic microspherical carbon particles obtained from polymerization of a

P. Lavela (✉) · F. Nacimiento · G. F. Ortiz · J. L. Tirado
Laboratorio de Química Inorgánica, Universidad de Córdoba,
Edificio C3, Campus de Rabanales,
14071 Córdoba, Spain
e-mail: iq1lacap@uco.es

mixture of resorcinol/formaldehyde have demonstrated to be suitable electrode materials for sodium ion cells [12]. Moreover, these carbon gels are promising materials for encasing metal powder because of the gelly-like texture of the departure precursor. Thus, containing silicon [13] and tin [14] based composite materials have been reported.

This paper reports the evaluation of Sn–Co–C composites prepared by carbothermal reduction of the metal oxides parallel to carbonization of a resorcinol–formaldehyde polymer. The aim was to evaluate the electrochemical behavior in lithium cells of tin–cobalt intermetallics when they are dispersed into a carbon matrix. The gel-like nature of the resorcinol–formaldehyde polymer may ensure a suitable embedding of the resulting alloy.

Materials and methods

The preparation of the Sn–Co–C composites was carried out by the impregnation of a homogeneous mixture of the metal oxides finely powdered in an organic gel formed by the resorcinol/formaldehyde method. For this purpose, commercial SnO_2 (Panreac) and CoO (Aldrich) in 95:5 and 85:15 molar ratios were ball-milled for 5 h at 300 rpm. For the preparation of the organic gel, 4.5 g of resorcinol were added to 6.5 mL of formaldehyde stabilized in methanol [Panreac, 37% (wt)] and 15 mL of distilled water under continuous stirring at room temperature. A volume of 60 mL of 0.035 M sodium carbonate solution was added to promote polymerization. After 1 h of stirring at room temperature, the aquagel was mixed with the metal oxides in the appropriated proportion to prepare several carbon to metal ratios. The content was transferred to a round-bottom flask and was refluxed at 85 °C for approximately 3 h. This was the time needed for a solid gel formation ensuring the homogenous mixture of carbonaceous and metal phases. Then, the gel was transferred in a closed glass flask and cured with acetone for 3 days at room temperature. The role of acetone was the gel dehydration; therefore, the solvent was replaced daily for an optimal operation. The solid gel was eventually filtered, washed, and then heated at 300 °C for 2 h. The composite precursor was ground and re-heated at 800 °C for 4 h under an argon stream in a tube furnace. The heating rate was 2.5 °C/min.

Two different Sn/Co molar ratios, henceforth referred to as 85:15, 95:5, and one tin-only composition, were selected for this study. For the 85:15 ratio, three different ratios between the metal oxides (MO_x=SnO_2+CoO) and resorcinol (R) masses were used in the synthesis. The resulting samples are referred to as MO_x/R and ratio took the following values: 0.3, 0.67, and 1.5. Additionally, a coke material prepared in the same conditions, but free of metal elements, was also prepared for comparison purposes.

X-ray diffraction (XRD) patterns were recorded in a Siemens D-5000 apparatus provided with CuKα radiation and graphite monochromator. The 2θ scan rate was 0.04° per 1.2 s. Scanning electron microscopy (SEM) images were obtained in a JEOL-SM6300 microscope provided by the Service of Support to Research at the University of Córdoba. The ^{119}Sn Mössbauer spectra (MS) were recorded at room temperature with an Ametek–Wissel constant-acceleration spectrometer in transmission mode. The source of radiation was ^{119m}Sn in a $BaSnO_3$ matrix. The isomer shift scale is set by using a $BaSnO_3$ pattern. The center of the peak of the Sn(IV) signal is established as the zero value of the scale. The spectra profile was decomposed in Lorentzian lines using a least-square-based method (F. Landry and P. Schaaf, WinISO—Windows Mössbauer Fitting 625 Programme, 1998, private communication). The goodness of the fit was controlled by the χ^2 value.

The electrochemical performance of the Sn–Co–C composites was evaluated by using two-electrode Swagelok-type cells. The assembly used 9-mm discs of lithium metal as counter electrodes. The working electrode was fabricated by mixing 92% of active material and 8% polyvinylidene difluoride binder. A paste was formed with that mixture and *n*-methyl pyrrolidinone and eventually deposited as a film on a cooper foil of the same diameter. Both electrodes were separated by a 1 M $LiPF_6$ (EC/DEC= 1:1) electrolyte solution that was supported in Whatman glass fiber discs. The assembly of test cells and handling of the discharged electrode was carried out in an MBraun glove box under an argon atmosphere. An Arbin potentiostat/galvanostat multichannel system was used to cycle galvanostatically the lithium cells at 20 mA/g rate for both charge and discharge branches. Electrochemical impedance spectroscopy was carried out in an Autolab PGSTAT12 system. Three-electrode lithium cells were used, providing a lithium metal disc as a reference electrode. The test cells were previously discharged using a MacPile system by step potential electrochemical spectroscopy. The scan rate was set at 10 mV/0.1 h. Before measuring the impedance values, the cells were kept in open circuit for at least 5 h to achieve a quasi-equilibrium system. An AC voltage signal of 5 mV was applied from 100 kHz to 2 mHz.

Results and discussion

XRD analysis

XRD patterns of the annealed samples are shown in Fig. 1. A set of narrow reflections could be ascribed to the presence of several tin-containing solids, including metallic phases such as tin (JCPDS 04-0673), $CoSn_2$ (JCPDS 25-0256), and CoSn (JCPDS 02-0559). Some oxide impurities

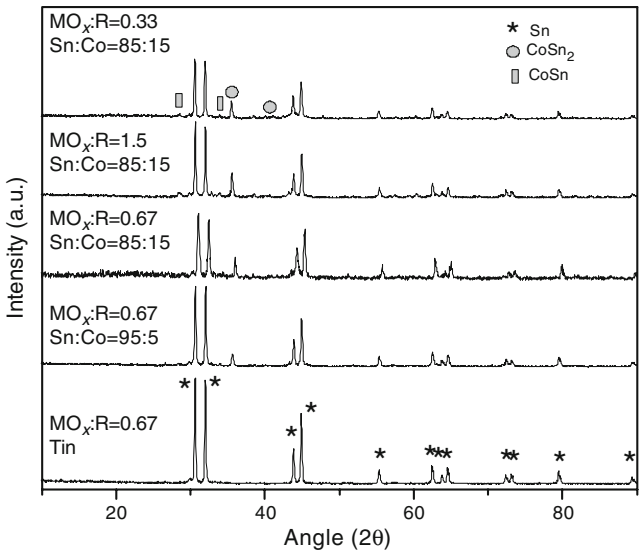

Fig. 1 X ray diffraction patterns of Sn–Co–C composites

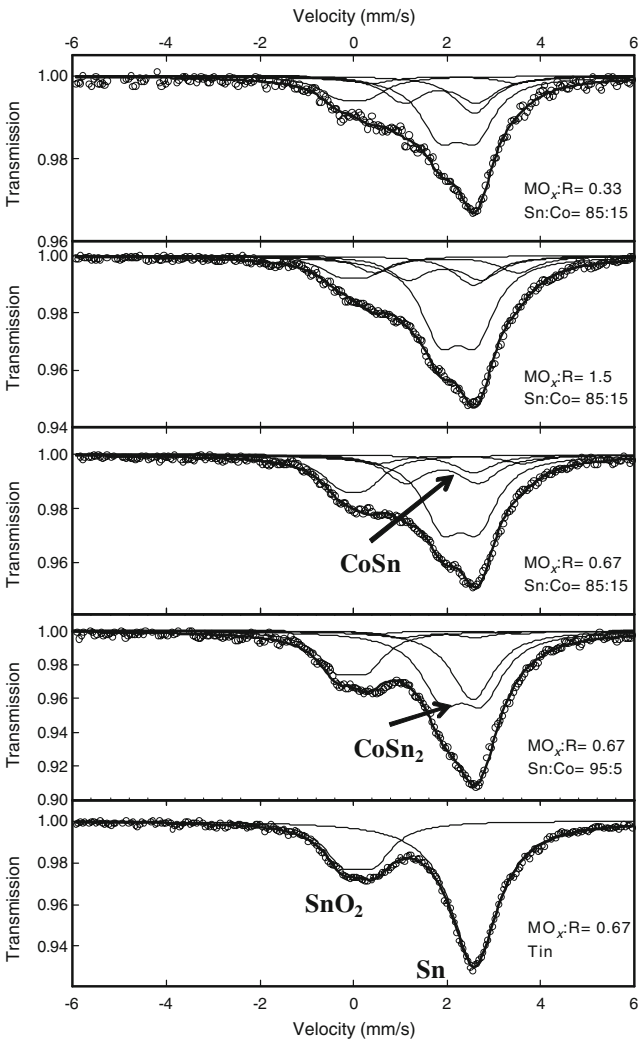

Fig. 2 ^{119}Sn Mössbauer spectra of Sn–Co–C composites

can be ascribed to either an incomplete reduction during the annealing process or to further surface oxidation. The selected annealing temperature prevented an appreciable structural ordering of the carbonaceous phase, and hence, reflections were not detected.

^{119}Sn Mössbauer spectroscopy

^{119}Sn Mössbauer spectroscopy is a useful tool to quantify the contribution of tin phases to the studied samples. Figure 2 shows the experimental spectra of the tin-containing phases and the Lorentzian signal profiles calculated from the fitting. The hyperfine parameters are written in Table 1. The cobalt-free sample showed two resolved signals located at the regions belonging to metallic tin and Sn(IV). According to the XRD pattern, they can be assigned to β-Sn and SnO_2. The presence of SnO_2 can be justified by a partial oxidation of the surface of tin particles. For samples containing cobalt, the spectrum profile progressively changes until it eventually becomes an asymmetric and highly broadened profile. This behavior is due to the occurrence of new bands at intermediate shifts. The overlapped signals are difficult to fit. To overcome this problem, the hyperfine parameters of CoSn and $CoSn_2$ phases were taken from the literature [15] and used as initial values in the fitting procedure. The most remarkable feature is the significant contribution of SnO_2, though it slightly decreased when cobalt and carbonaceous proportion was augmented. This fact evidences the important role of carbon material in the reduction of the initial oxides. In addition, the reactivity of cobalt to form alloys with tin is revealed by the abrupt decrease of β-tin contribution when cobalt content is increased. This effect is parallel to the increasing contribution of cobalt–tin phases.

Electron microscopy

The morphological properties of these samples were evaluated from the SEM micrographs. Figure 3a shows a close view of sample-only containing tin. Spherical particles of tin, with diameter values ranging from some tenth to several micrometers, are mainly decorating the surface of the carbon substrate. When cobalt atoms are present in the composition, the population of surface particles is drastically reduced. Agglomerates of nanometric particles are mostly embedded in the carbonaceous matrix. The influence of cobalt atoms to provide strong links between tin and carbon that improves the stability of the composite material has been reported [16].

Table 1 Hyperfine parameters of the deconvoluted Mössbauer spectra

Sample	s/d	Tin phase	δ (mm/s)	Δ (mm/s)	Γ (mm/s)	C (%)	χ^2
MO_x/R=0.67 Tin only	d	SnO_2	0.10 (3)	0.66 (2)	0.98 (4)	28.1	0.738
	s	β-Sn	2.58 (1)	–	1.2 (1)	71.9	
MO_x/R=0.67 Sn/Co=95:5	d	SnO_2	−0.04 (4)	0.65 (3)	0.96 (5)	21.5	0.670
	s	β-Sn	2.55 (1)	–	1.1 (2)	26.7	
	d	CoSn	1.82 (1)	1.57 (1)	1.1 (1)	4.4	
	d	CoSn	2.038 (1)	3.08 (2)	1.1 (1)	2.2	
	d	$CoSn_2$	2.32 (1)	0.86 (2)	1.1 (2)	45.2	
MO_x/R=0.67 Sn/Co=85:15	d	SnO_2	0.00 (2)	0.54 (3)	1.0 (2)	18.7	0.551
	s	β-Sn	2.57 (1)	–	1.1 (2)	7.0	
	d	CoSn	1.89 (2)	1.56 (1)	1.1 (1)	20.3	
	d	CoSn	2.08 (5)	3.06 (1)	1.1 (1)	6.7	
	d	$CoSn_2$	2.28 (1)	0.77 (1)	1.1 (2)	47.4	
MO_x/R=1.5 Sn/Co=85:15	d	SnO_2	0.00 (3)	0.60 (5)	1.0 (2)	10.9	0.696
	s	β-Sn	2.57 (1)	–	1.0 (2)	10.4	
	d	CoSn	1.95 (2)	1.56 (1)	1.0 (1)	16.0	
	d	CoSn	1.98 (4)	3.06 (1)	1.0 (1)	11.8	
	d	$CoSn_2$	2.23 (1)	0.77 (1)	1.0 (2)	50.9	
MO_x/R=0.33 Sn/Co=85:15	d	SnO_2	0.00 (4)	0.63 (7)	1.0 (2)	14.1	0.502
	s	β-Sn	2.57 (1)	–	1.0 (2)	15.4	
	d	CoSn	1.86 (3)	1.56 (3)	1.0 (1)	20.9	
	d	CoSn	2.0 (1)	3.06 (1)	1.0 (1)	5.8	
	d	$CoSn_2$	2.22 (2)	0.77 (1)	1.0 (1)	43.8	
MO_x/R=0.67 Sn/Co=85:15 Disch. to 0 V	s	β-Sn	2.65 (2)	–	1.0 (1)	22.6	0.338
	d	$Li_{22}Sn_5$	1.79 (2)	0.24 (1)	0.94 (1)	38.7	
	d	$Li_{22}Sn_5$	1.82 (2)	0.94 (1)	0.94(1)	38.7	

s/d singlet (*s*) or doublet (*d*), δ isomeric shift, Δ quadrupolar splitting, Γ line-width at half maximum, C contribution/concentration, χ^2 goodness of the fitting

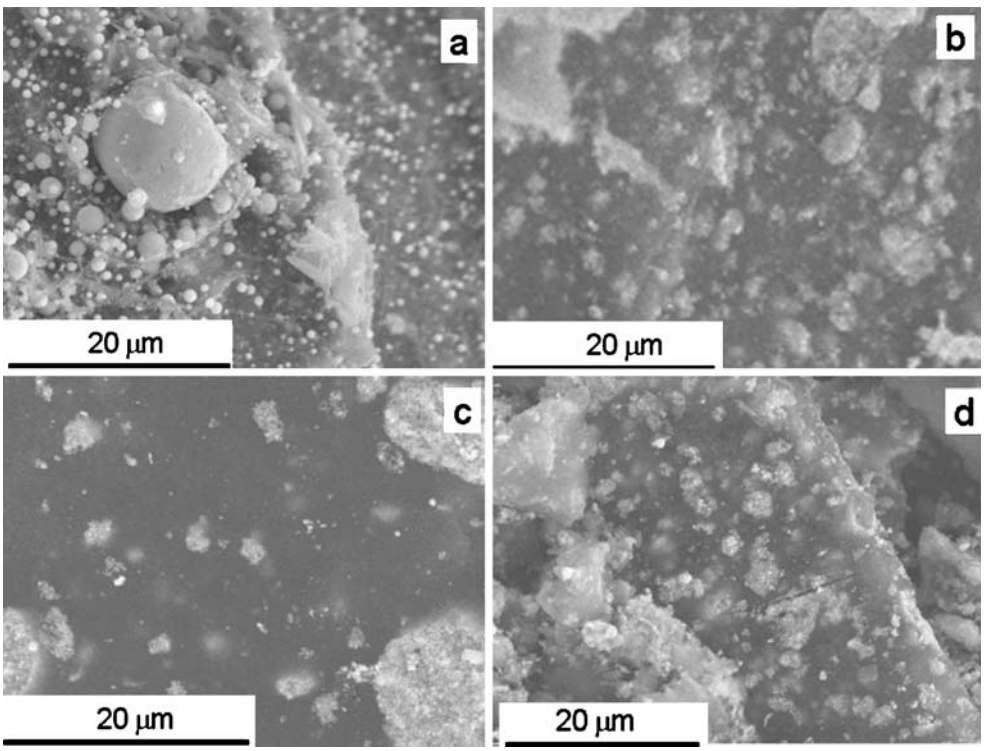

Fig. 3 SEM micrographs of metal–carbon composites (**a**) tin-only sample (MO_x/R=0.67); **b** Sn:Co=95:5 (MO_x/R=0.67); **c** Sn/Co=85:15 (MO_x/R=0.67); **d** Sn/Co=85:15 (MO_x/R=1.5)

Electrochemical performance

Figure 4 shows the intensity versus voltage plots for the first few cycles of lithium test cells using composites prepared with different Sn/Co and/or MO_x/R ratios. The first discharge profile differs from subsequent discharges. It is assigned to the drastic structural and morphological changes occurring upon alloy formation that cannot be recovered after the first discharge. Therefore, the new sites for the reaction with lithium possess quite different energy what is reflected in the profile of the second discharge. The contribution of the irreversible reduction of SnO_2 phase, at 0.9 V, was negligible in all cases. The observed bands in the discharge and charge curves correspond to the reversible formation of Li–Sn alloys. The enhanced broadening of the bands would be indicative of low crystalline domains achieved by the dispersion effect of the carbon matrix during the carbothermal reaction. For the samples with Sn/Co=85:15, a decrease in the MO_x/R ratio (Fig. 4a–c) led to the decrease of the intensity of the alloy main signal. This behavior is in contrast with the higher contribution of lithium insertion in the carbon material occurring in the 0–0.2 V range.

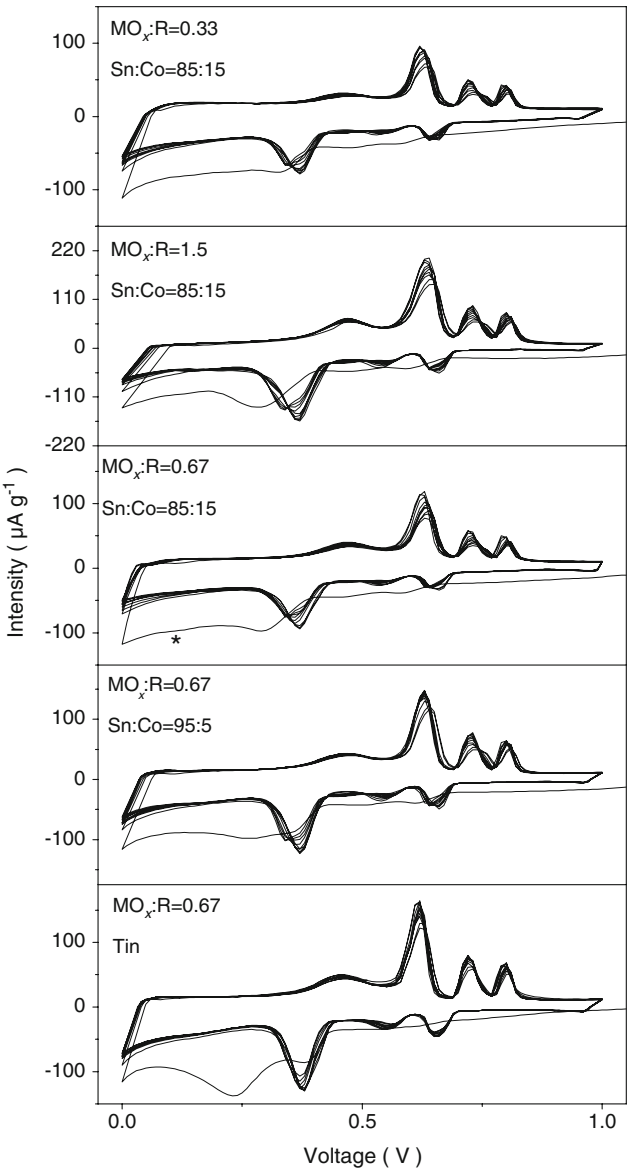

Fig. 4 Intensity versus voltage plots recorded by step potential electrochemical spectroscopy. **a** Sn/Co=85:15 (MO_x/R=0.33); **b** Sn/Co=85:15 (MO_x/R=1.5); **c** Sn/Co=85:15 (MO_x/R=0.67). **d** Sn/Co=95:5 (MO_x/R=0.67); **e** tin only. Scan rate, 10 mV/0.1 h

On decreasing the cobalt content (Fig. 4c–e), the main reduction peak at approximately 0.25 V is shifted to approximately 0.3 V, while a new highly broadened band is observed at approximately 0.1 V (marked with an asterisk). It has been reported that the occurrence of cobalt–tin alloys induces a diminution of the working potential in the main alloying plateau [17]. Hence, the latter signal could be assigned to the increased contribution of these phases when cobalt content is increased. This signal disappeared on subsequent cycling, and hence, an electrochemical reaction between Li and Sn can be inferred for a long-term cycling.

To unfold the nature of the tin phases yielded by the discharging process, the ^{119}Sn Mössbauer spectrum of a fully discharged electrode was recorded at room temperature (Fig. 5). The asymmetric signal could be decomposed in several components ascribable to $Li_{22}Sn_5$ and β-Sn (Table 1). Different reports have evaluated the ex situ ^{119}Sn MS of Sn-based intermetallic materials such as $CoSn_2$ [18], Ni_3Sn_4 [18], and Cu_6Sn_5 [19] when used as working electrodes in lithium cells. In these cases, the occurrence of the Li-rich Li_7Sn_2 alloy at the end of the first discharge was reported. In contrast, a recent study on CoSn revealed that no Li_xSn phases were detectable by XRD or Mössbauer spectroscopy [20]. Thus, the absence of signals

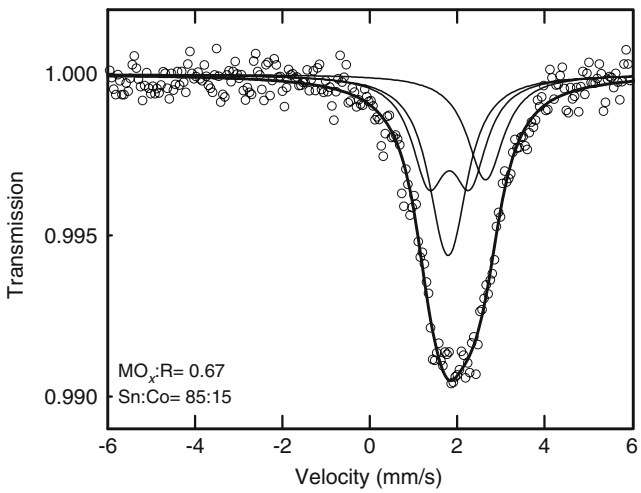

Fig. 5 ^{119}Sn Mössbauer spectrum of a fully discharged electrode with Sn/Co=85:15 and a MO_x/R=0.67 ratio

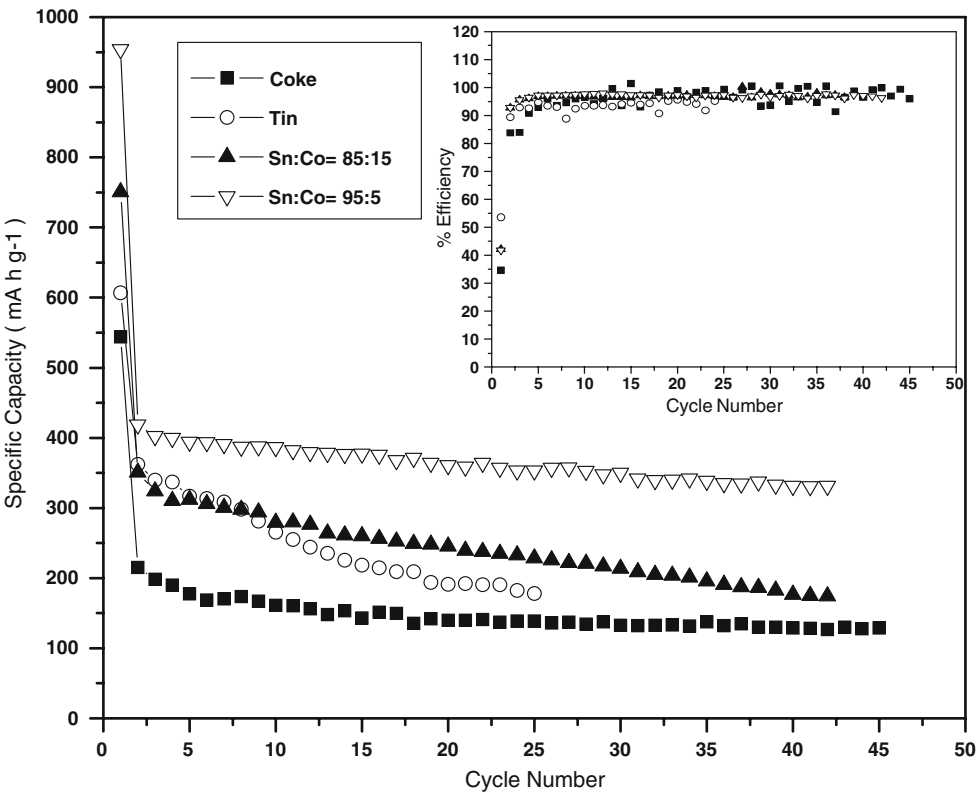

Fig. 6 Galvanostatic cycling of Sn–Co–C composites prepared with a metal/carbon ratio equivalent to $MO_x/R=0.67$ and different contents of cobalt in their composition. *Inset* Plot of coulombic efficiency for the same range of cycles. Kinetic rate, 20 mA/g

corresponding to non-reacted Co–Sn alloys could be indicative of a higher reactivity of these intermetallic compounds as compared to tin metal. Nevertheless, its contribution to the $Li_{22}Sn_5$ cannot be established unequivocally. The presence of non-reacted tin at the end of the discharge can be attributed to kinetic factors contributing to the polarization of the discharge branch. This fact would justify their enhanced performance as electrode materials in lithium cells.

Figure 6 shows the discharge capacity values of lithium test cells assembled using samples with different metal contents. The cells were galvanostatically cycled between 0.02 and 1.0 V. The introduction of tin led to an important increase of the reversible capacity as expected from the significant contribution of Li_xSn alloys formation. Furthermore, an increase of the irreversible capacity in the first discharge is observed (inset in Fig. 6). Likely, tin phases also contribute to the initial irreversibility. Thus, a non-negligible contribution of SnO_2 was observed in the MS (Fig. 2). Moreover, the significant changes between the profile of the first and second discharges, mainly in the region of lithium–tin alloy formation, may involve additional irreversible reactions to that expected from solid electrolyte interphase (SEI) formation on the carbon surface. On the other hand, some authors have attributed the enhanced initial coulombic efficiency to the nano-tin-induced decomposition of the $ROCO_2Li$ species in the SEI layer [21]. However, it is has been reported that the introduction of tin particles plays an important role on the cyclability upon alloying and de-alloying with lithium. Thus, tin particles confined within the carbon micropores exhibit better performance, since the detrimental effect of the volume expansion is avoided [22]. Unfortunately, the capacity retention was very poor, even if the upper cut off voltage was selected at 1 V to avoid deleterious structural and morphological changes [23]. The introduction of cobalt contributed to improve both capacity and cyclability. Only minor cobalt contents (Sn/Co=95:5) were able to improve the capacity retention as compared to the cobalt-free sample. Capacity values higher than 330 mAh/g were maintained after more than 30 cycles. This result evidences the efficiency of this transition metal to enhance the electrochemical reactivity of the composite. A further increase of the cobalt content (Sn/Co=85:15) did not cause an improvement of the overall capacity. The lack of reactivity versus lithium is responsible for the increase of non-active electrode material. Nevertheless, the response could be improved if the MO_x/R ratio is allowed to increase.

In order to determine the influence of the carbon matrix on the electrochemical performance, the samples with the Sn/Co=85:15 ratio and different MO_x/R ratios were also cycled. Figure 7 shows a decrease in capacity of the first discharge attributable to the lesser molar capacity of carbon as compared to tin. This fact affected to subsequent cycles, and hence, the sample with higher carbon content (lower

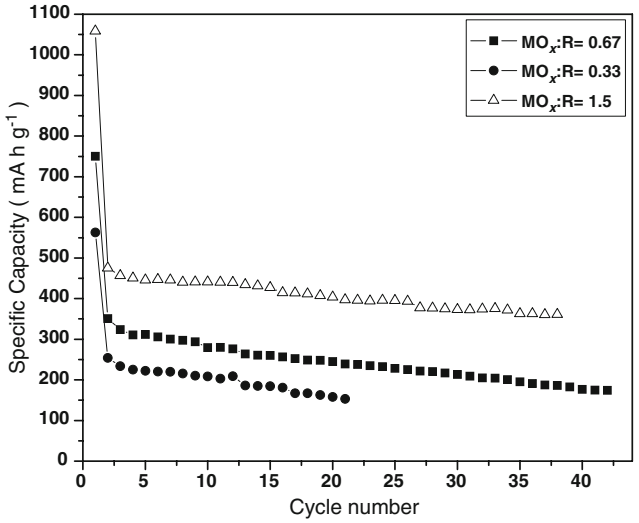

Fig. 7 Galvanostatic cycling of Sn–Co–C composites prepared with a Sn/Co=85:15 metal ratio and different MO_x/R ratios (MO_x/R=0.33, 0.67 and 1.5). Kinetic rate, 20 mA/g

ratio, MO_x/R=0.33) delivered the lowest capacities in the whole range. In turn, an increase of the tin content positively contributed to improve both capacity values and retention. A high reversible capacity value (475 mAh/g) was reached in the second cycle. Capacity values higher than 380 mAh/g were maintained after more than 30 cycles.

Electrochemical impedance spectroscopy

Electrochemical impedance spectroscopy provides interesting information concerning the kinetic properties of those electrode/electrolyte interphases playing a significant role in lithium migration. Nyquist plots of selected samples are included in Fig. 8a. The common profile is characterized by two depressed semicircles at high and intermediate frequencies and a straight line at low frequencies. The semicircles are respectively attributed to the kinetic barriers imposed to lithium migration through the SEI film and charge transfer occurring on the electrode surface. Moreover, the line observed at low frequencies corresponds to

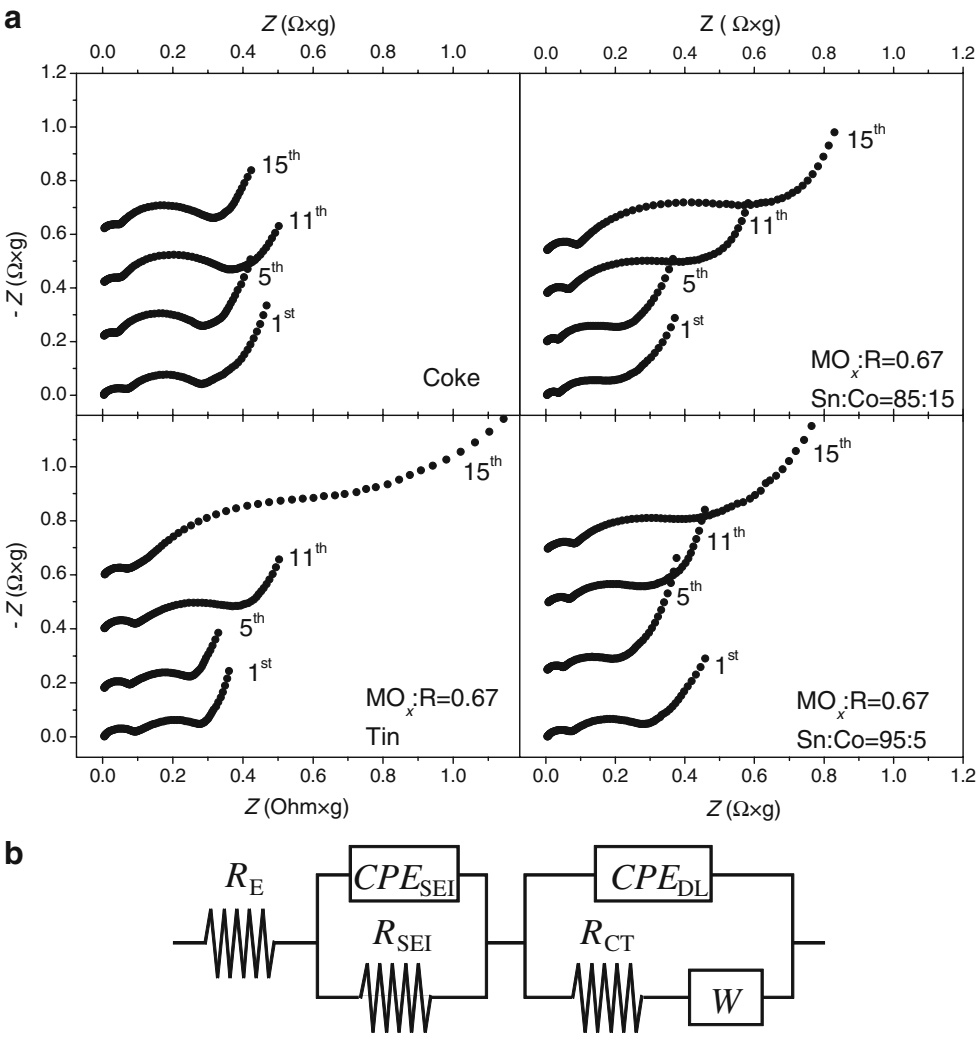

Fig. 8 **a** Nyquist plots fully discharged electrodes on the first, fifth, 11th, and 15th cycles. **b** Equivalent circuit used for the fitting of the spectra

lithium diffusion into the electrode material [24, 25]. The overall impedance was kept almost constant for the coke material on cycling. This result differs from previous reported data on sulfur-containing vacuum residua in which an important increase of impedance was monitored. In the latter case, the presence of significant sulfur content was considered detrimental for the electrochemical behavior [26]. The inclusion of tin in the composite provoked a huge increment of the impedance for a large number of cycles. Likely, the volume expansion induced by the reversible alloy formation may contribute to a loss of electrical connectivity among particles during a repeated cell operation.

The introduction of cobalt in the composite stoichiometry, even at low concentrations, led to a significant decrease of the impedance during cycling. This fact evidences that the beneficial effect of low cobalt contents can be attributed to kinetic effects. In order to determine the specific influence of the interphases, several examples of equivalent circuits have been proposed in the literature [27, 28]. In this work, the resistance values were calculated from the fitting of the spectra to the selected equivalent circuit displayed in Fig. 8b. In the used circuit, the migration phenomena described above are taken into the necessary account.

Figure 9 plots the resistance values (R_{SEI} and R_{CT}) versus cycle number. Although, R_{SEI} values did not reach values higher than 0.11 Ωg in the measured range, a clear tendency could not be inferred. The instability of SEI films on both graphitized materials [29] and cokes [30] as a result of impedance measurements has been reported. Most likely,

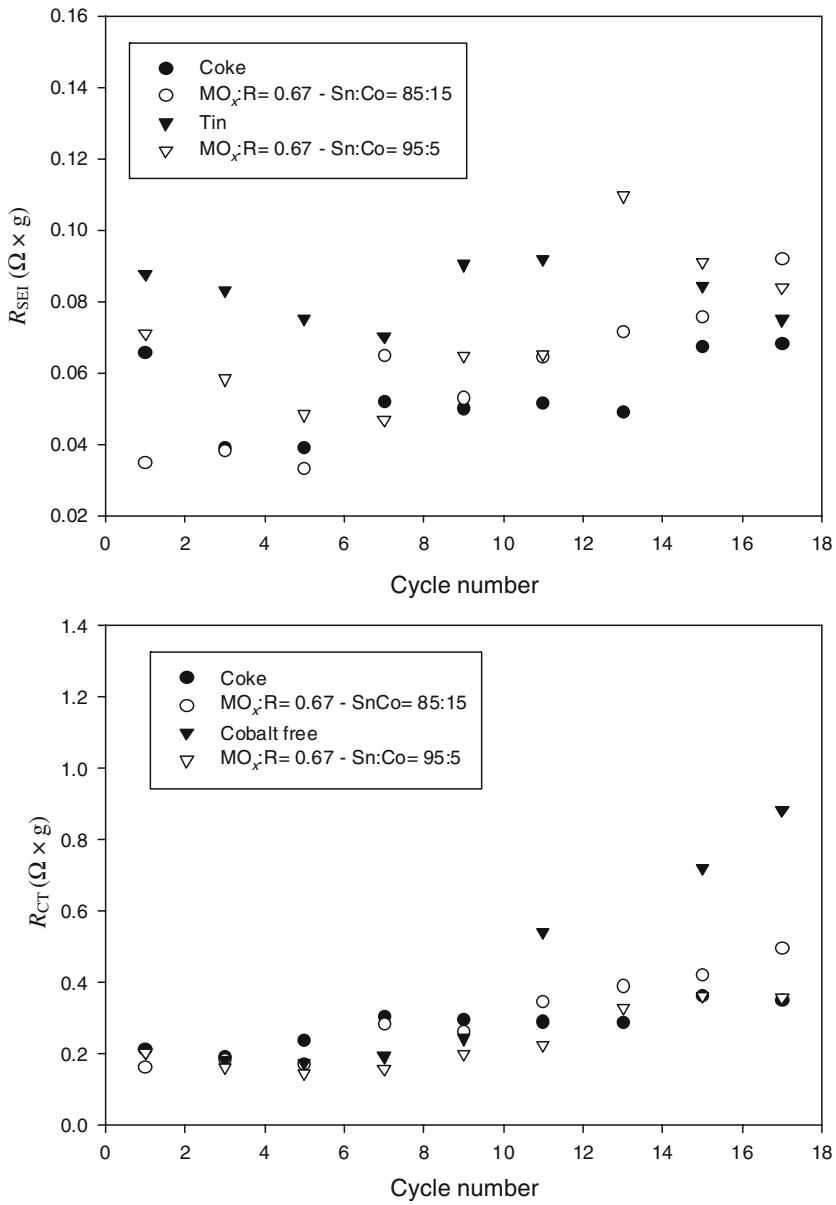

Fig. 9 Resistance versus cycle number plots of coke, tin only, Sn/Co=95:5 (MO_x:R=0.67) and Sn/Co=85:15 (MO_x/R=0.67)

the erratic behavior of the SEI values in Fig. 9 could be ascribed to the presence of dislodge passivation debris migrating cataphoretically.

Otherwise, charge transfer resistance steadily increased in cycling for coke and Sn–Co–C composites. Contrarily, an enhanced increase of resistance was recorded for the cobalt-free sample. This result would indicate an important charge accumulation on the electric interphase. In turn, this is likely due to a significant decrease in the electrical conductivity during cycling.

Conclusions

The resorcinol/formaldehyde polymerization–carbonization plus carbothermal reduction process has been used to prepare Sn–Co–C composites. For this purpose, finely powdered tin and cobalt oxides were embedded in the organic gel like precursor. Highly dispersed tin and cobalt–tin phases were eventually obtained by carbothermal reaction after carbonization of the composite precursors. SEM images revealed the presence of carbonaceous particles with metal agglomerates homogeneously dispersed, either decorating the surface or embedded in the carbonaceous matrix. The effective reduction of metal oxides was verified by the XRD technique, in which tin and cobalt–tin phases were predominant.

^{119}Sn Mössbauer spectroscopy evidences the high contribution of cobalt–tin alloys in the initial composites. However, the discharge process involved the disappearance of these phases in further cycling as monitored by step potential electrochemical measurements and ex situ ^{119}Sn Mössbauer spectroscopy of a fully discharged electrode.

Nevertheless, the beneficial effect of the presence of cobalt was detected on a galvanostatic cycling and impedance measurements even with small amounts of cobalt added. The sample with Sn/Co=95:5 was able to improve the retention, as compare with tin-only composites. Capacity values around 330 mAh/g after 30 cycles were recorded. In contrast, only 140 and 191 mAh/g were, respectively, measured for coke and cobalt-free samples. This fact would indicate that the presence of crystalline or well-formed cobalt–tin phases is not essential for an improvement of the electrochemical performance of the metal carbon composite. Cobalt plays a determining effect even in amorphous domains and relatively small quantities.

However, the moderated capacity values recorded in this study demanded a new strategy in order to achieve more performing results. An increase of the MO_x/R ratio on the Sn/Co=85:15 ratio led to higher reversible capacity values of 380 mAh/g after 30 cycles.

The kinetic response of the electrode materials was determined by impedance measurements. The cobalt-containing composites showed a lower increase in charge transfer resistance as compared to the cobalt-free samples. Therefore, the kinetic component seems to play an important role in the improvement of capacity retention observed in Sn–Co–C composites.

Acknowledgments The authors are grateful to MEC for financial support (Contract PET2005_0670_01). We also thank to M.C. Mohedano for her technical support and the Central Services of the University of Córdoba, especially to F. Gracia for the use of the SEM microscope. F. Nacimiento is indebted to MEC for his predoctoral grant. G.F. Ortiz is indebted to FQM-1447.

References

1. Tirado JL (2003) Mater Sci Eng Rep 40:103 doi:10.1016/S0927-796X(02)00125-0
2. Manev V, Naidenov I, Puresheva B, Zlatilova P, Pistoia G (1995) J Power Sources 55:211 doi:10.1016/0378-7753(95)02192-J
3. Ohzuku T, Iwakoshi Y, Sawai K (1993) J Electrochem Soc 140:2490 doi:10.1149/1.2220849
4. Menachem C, Wang Y, Flowers J, Peled E, Greenbaum SG (1998) J Power Sources 76:180 doi:10.1016/S0378-7753(98)00167-0
5. Nakajima T, Koh M, Singh RN, Shimada M (1999) Electrochim Acta 44:2879 doi:10.1016/S0013-4686(99)00048-1
6. Idota Y, Kubota T, Matsufuji A, Maekawa Y, Miyasaka T (1997) Science 276:1395 doi:10.1126/science.276.5317.1395
7. Alcantara R, Fernandez-Madrigal FJ, Lavela P, Tirado JL, Jumas JC, Olivier-Fourcade J (1999) J Mater Chem 9:2517 doi:10.1039/a902060h
8. Todd ADW, Mar RE, Dahn JR (2006) J Electrochem Soc 153: A1998 doi:10.1149/1.2257985
9. Hassoun J, Ochal P, Panero S, Mulas G, Bonatto Minella C, Scrosati B (2008) J Power Sources 180:568 doi:10.1016/j.jpowsour.2008.01.059
10. Ferguson PP, Todd ADW, Dahn JR (2008) Electrochem Commun 10:25–31 doi:10.1016/j.elecom.2007.10.025
11. Trifonova A, Winter M, Besenhard JO (2007) J Power Sources 174:800 doi:10.1016/j.jpowsour.2007.06.229
12. Alcantara R, Lavela P, Ortiz GF, Tirado JL (2005) Electrochem Solid St 8:A222 doi:10.1149/1.1870612
13. Hasegawa T, Mukai SR, Shirato Y, Tamon H (2004) Carbon 42:2573 doi:10.1016/j.carbon.2004.05.050
14. Wang K, He X, Ren J, Wang L, Jiang C, Chunrong W (2006) Electrochim Acta 52:1221 doi:10.1016/j.electacta.2006.07.020
15. Jaén J, Varsányi ML, Kovács E, Czakó-Nagy I, Buzás A, Vértes A, Kiss L (1984) Electrochim Acta 29:1119 doi:10.1016/0013-4686(84)87164-9
16. Inoue H (2006) High capacity negative electrode materials next to carbon; Nexelion. Proceedings of the International Meeting on Lithium Batteries. The Electrochemical Society, Biarritz, France
17. Dahn JR, Mar RE, Abouzeid A (2006) J Electrochem Soc 153: A361 doi:10.1149/1.2150160
18. Naille S, Jumas JC, Lippens PE, Olivier-Fourcade J (2008) J Power Sources (in press) doi:10.1016/j.jpowsour.2008.07.058
19. Choi W, Lee JY, Lim HS (2004) Electrochem Commun 6:816 doi:10.1016/j.elecom.2004.05.018
20. Alcántara R, Rodríguez I, Tirado JL (2008) ChemPhysChem 9:1171 doi:10.1002/cphc.200800031

21. Guo B, Shu J, Tang K, Bai Y, Wang Z, Chen L (2008) J Power Sources 177:205 doi:10.1016/j.jpowsour.2007.11.003
22. Grigoriants A, Soffer G, Salitra D, Aurbach D (2005) J Power Sources 146:185 doi:10.1016/j.jpowsour.2005.03.120
23. Courtney IA, Dahn JR (1997) J Electrochem Soc 144:2943 doi:10.1149/1.1837941
24. Aurbach D, Gnanaraj JS, Levi MD, Levi EA, Fischer JE, Claye A (2001) J Power Sources 97–98:92 doi:10.1016/S0378-7753(01)00594-8
25. Wang C, Appleby AJ, Little FE (2002) J Electrochem Soc 149:A754
26. Tirado JL, Santamaría R, Ortiz GF, Menéndez R, Lavela P, Jiménez-Mateos JM, Gómez García FJ, Concheso A, Alcántara R (2007) Carbon 45:1396
27. Funabiki A, Inaba M, Ogumi Z, Yuasa S, Otsuji J, Tasaka A (1998) J Electrochem Soc 145:172 doi:10.1149/1.1838231
28. Wang C, Appleby AJ, Little FE (2002) J Electrochem Soc 149:A754
29. Aurbach D, Markovsky B, Levi MD, Levi E, Schechter A, Moshkovich M, Cohen Y (1999) J Power Sources 81–82:95
30. Avery NR, Black KJJ (1997) Power Sources 68:191 doi:10.1016/S0378-7753(96)02550-5